



ELSEVIER

Available online at www.sciencedirect.com

SCIENCE @ DIRECT®

Earth and Planetary Science Letters 6702 (2003) 1–10

EPSL

www.elsevier.com/locate/epsl

Southern Ocean sea ice and radiocarbon ages of glacial bottom waters

A. Schmittner^{1,*}*Max-Planck-Institut für Biogeochemie, P.O. Box 10 01 64, 07701 Jena, Germany*

Received 27 January 2003; received in revised form 14 May 2003; accepted 20 May 2003

Abstract

Analyzing simulations of glacial ocean circulation and radiocarbon distribution I show that increased sea ice cover over the Southern Ocean reduces ventilation and radiocarbon content of the deep ocean. Two simulations, one present-day and one glacial, tuned to have similar rates of North Atlantic Deep Water formation are used. Insulation from air–sea gas exchange due to more extended sea ice cover increases Southern Ocean radiocarbon ages by more than 100 yr. Higher rates of sea ice formation and export from high southern latitudes lead to a salinification of Antarctic Bottom Water (AABW), making it the most saline deep water mass of the glacial world oceans. This increases the density of AABW and hence its rate of formation. Mass and radiocarbon fluxes to the deep ocean are thus decoupled. Both older Southern Ocean waters and a stronger flux of AABW increase radiocarbon ages of glacial bottom waters by up to 300 yr. Available reconstructions of glacial bottom water properties are broadly consistent with the simulation. These results question previous inferences from radiocarbon distributions on glacial deep water formation rates.

© 2003 Published by Elsevier Science B.V.

Keywords: Last Glacial Maximum; Southern Ocean; sea ice; radiocarbon age; deep water

1. Introduction

From the interpretation of different tracer distributions it has been suggested that the strength

of North Atlantic Deep Water (NADW) formation during the Last Glacial Maximum (LGM) was considerably weaker than it is today. The tracers applied to this problem are nutrient proxies like $\delta^{13}\text{C}$ [1] and Cd/Ca ratios [2], but also radiocarbon ($\delta^{14}\text{C}$) [3]. Although all of these tracers seem to be consistent with a reduced circulation it has been criticized that changes in the mass flux cannot be unequivocally inferred from changed tracer distributions [4,5]. Here I analyze detailed simulations of radiocarbon distribution in the glacial ocean in the context of this debate.

Broecker et al. [3] inferred from radiocarbon measurements in benthic and planktonic forami-

* Tel.: +49-431-880-7324; Fax: +49-431-880-1569;

<http://www.passagen.uni-kiel.de/people/as>.

E-mail address: andreas@passagen.uni-kiel.de

(A. Schmittner).

¹ Present address: Institut für Geowissenschaften, Christian-Albrechts-Universität Kiel, Olshausenstrasse 40, 24118 Kiel, Germany.

nifera that glacial deep waters in the North Atlantic were 600–700 yr old, whereas at present they are only 300–400 yr. From this observation they concluded that NADW flow must have been weaker during the LGM. Recently, however, a modeling study [6] showed that Broecker's data are consistent with a circulation strength similar to today. Here I will show that increased sea ice cover in the glacial Southern Ocean leads to older radiocarbon ages of deep waters in the Atlantic even for unchanged deep water formation in the North Atlantic. The aim of the present paper is not a realistic simulation of the LGM but rather to illustrate the effect of increased sea ice on glacial bottom waters and to provide a first quantification of its magnitude.

2. Model description

The model and simulations I analyze below are described in detail elsewhere [6,7]. Here I only provide a brief summary. The oceanic component is a fully three-dimensional non-linear general circulation model of the world's oceans [8] with isopycnal mixing and a parameterization of the effect of eddy-induced tracer transport [9]. It is coupled to a single-level energy–moisture balance model of the atmosphere and a dynamic–thermodynamic sea ice component. Air–sea heat and gas exchange (i.e. of radiocarbon) is inhibited if sea ice is present. As sea ice concentration reaches 100%, gas exchange approaches zero. Hence, unresolved fluxes through leads or polynias are not taken into account. Diapycnal diffusivities range from $0.6 \text{ cm}^2/\text{s}$ near the surface to $1.6 \text{ cm}^2/\text{s}$ at 5000 m depth. The seasonal cycle is resolved while the model does not exert higher frequency and inter-annual variability. Differences between glacial and modern simulations are prescribed CO_2 , orbital parameters and ice sheets. Note that for both glacial and modern simulations prescribed present-day (PD) wind velocities are used for the momentum transfer to sea ice and for the advection of atmospheric moisture. For general model details the reader is referred to [7].

Radiocarbon is introduced as a passive tracer with a half-life of 5730 yr [10]. A non-wind speed-

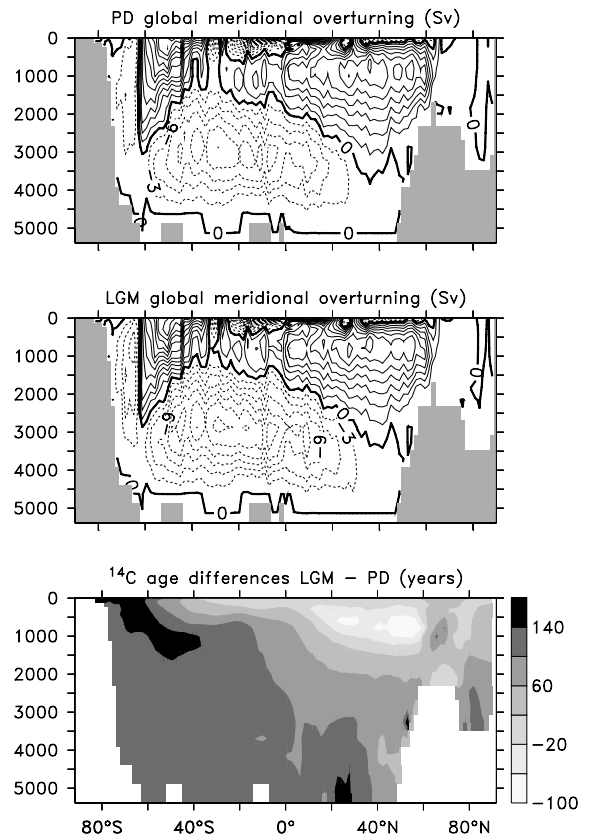


Fig. 1. Latitude–depth sections of global Eulerian (advects velocity) mass stream function for the PD (top) and glacial (middle) simulation. Isoline difference is 3 Sv. The models are tuned to have similar rates of NADW formation. Note that AABW formation is slightly increased in the glacial simulation. The bottom panel shows differences in global zonal mean radiocarbon ages with respect to atmospheric ^{14}C . Deep waters in the glacial simulation are more than 100 radiocarbon years older than in the PD simulation due to decreased ventilation of the Southern Ocean.

dependent parameterization of the air–sea gas exchange (equation A2 in [11]) with a relaxation time τ of 5 yr is used. Further details concerning the implementation of radiocarbon and comparison with modern and LGM observations in the Atlantic can be found elsewhere [6].

In the following, an analysis from two near-equilibrium simulations (1500 yr with fixed forcing, total integration time is much longer) is presented that are described in detail in [6]. The PD simulation was termed ‘PD eq 1700’ in [6] and the LGM simulation was termed ‘LGM eq 500’.

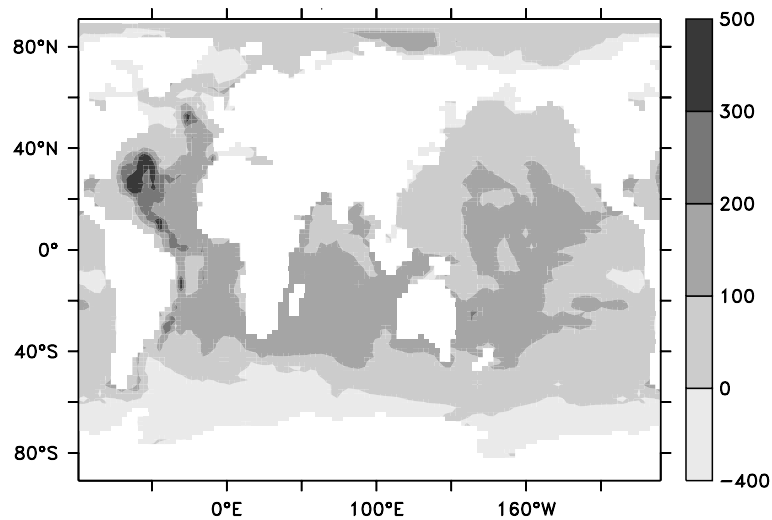


Fig. 2. Change in top-to-bottom radiocarbon age difference in yr between LGM and PD simulation.

These simulations are tuned by prescribed alterations of the North Atlantic freshwater balance to have nearly identical rates of NADW formation (22.6 for PD, 22.3 for the LGM, see Fig. 1 for global stream function). This excludes changes in NADW from simulated differences in glacial deep water properties. Note that I do not claim that NADW formation at the LGM was similar to today. Rather, I use these simulations in order to illustrate ventilation changes *not* caused by differences in NADW formation rate.

3. Model results

In the North Atlantic a southward shift of convection sites leads to younger glacial ^{14}C ages between 40°N and 60°N at 500–1000 m depth (Fig. 1). The largest radiocarbon age differences between the two runs, however, occur at the high-

latitude Southern Ocean. In the glacial simulation waters are more than 100 yr older than at PD. Maxima of more than 140 yr at the surface south of 60°S are advected north between 1000 and 1500 m depth with Antarctic Intermediate Water. Older bottom water masses are also transported towards lower latitudes and increase radiocarbon ages in all basins below 1500 m. Older Southern Ocean waters and a slightly enhanced flux of Antarctic Bottom Water (AABW) lead to larger age differences between bottom and surface water masses at all latitudes north of about 60°S (Fig. 2). In the western subtropical North Atlantic top-to-bottom age differences increase by more than 300 yr. In the tropical Atlantic the modeled increase by 40–260 yr (Table 1) is consistent with the observations by [3]. Note, however, that more recent data suggest that, at least for some events during the LGM, bottom waters in the North Atlantic were much older [12]. This would imply

Table 1
Tropical Atlantic radiocarbon ages (yr) with respect to the surface layer (top-to-bottom age differences)

Site	PD	LGM	Δ age
Carribean (79°W , 12°N , 1800 m)	284 (300)	324 (195 ± 140)	40 (-105 ± 140)
Ceara Rise (43°W , 4°N , 2800 m)	290 (350)	445 (780 ± 220)	155 (430 ± 220)
Ceara Rise (43°W , 4°N , 3500 m)	455 (350)	717 (600 ± 105)	262 (250 ± 105)
Ceara Rise (43°W , 4°N , 4000 m)	705 (400)	892 (705 ± 150)	187 (305 ± 150)

In parentheses, reconstructions from [3].

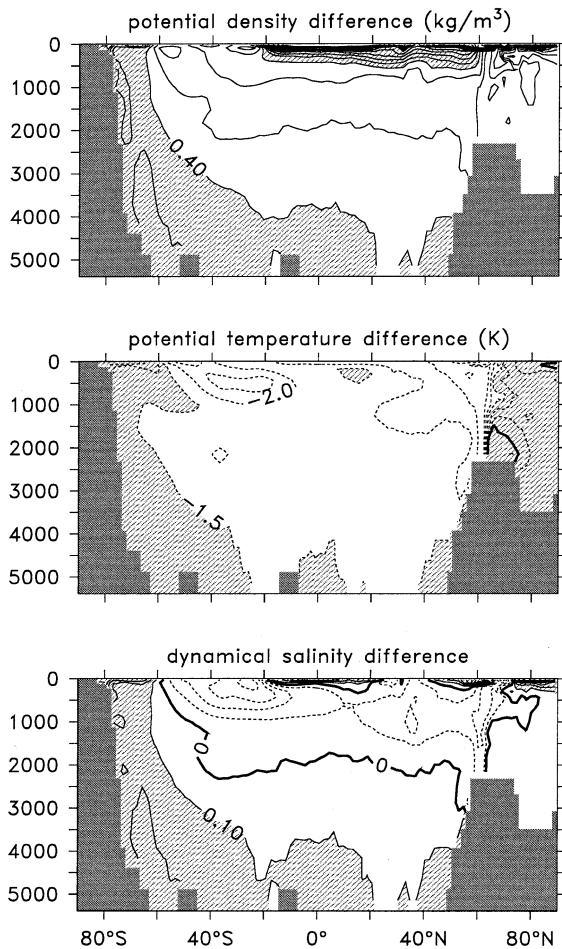


Fig. 3. Global zonally averaged differences in potential density (top panel, isoline difference 0.05 kg/m^3), potential temperature (middle panel, isoline difference 0.5 K) and dynamical (global mean values subtracted) salinity (bottom panel, isoline difference 0.1 salinity units) between glacial and PD simulation. Shaded are waters which increased more than 0.4 kg/m^3 in density, less than 1.5 K in temperature and more than 0.1 units in salinity.

an additional reduction in ventilation either through enhanced AABW formation or through reduced NADW formation or both. For a more detailed comparison with Atlantic observations the reader is referred to [6].

Bottom waters of southern origin are also heavier by more than 0.4 kg/m^3 (Fig. 3), leading to increased stratification of the global deep ocean below about 1000 m and to an increased rate of AABW formation (by about $4\text{--}5 \text{ Sv}$; see Fig. 1).

The minimum of the stream function below 2000 m (south of 60°S) decreased from -14.5 to -18.6 Sv (-6.2 to -11 Sv). The increased density of AABW is mainly caused by salinity. The dynamical salinity increased by more than 0.1 units south of 60°S , whereas upper ocean waters north of that latitude got fresher. Temperature changes are larger at low latitudes and smaller at high latitudes, where the cooling is limited by the freezing point. Changes in salinity lead to an increased global stratification, whereas changes in temperature are more vertically uniform.

Sea ice concentration has considerably increased in the glacial simulation (Fig. 4). Particularly between 50°S and 65°S concentrations increased by $20\text{--}50\%$ in area. The modeled winter sea ice edge, computed as the latitude of 10% sea ice cover, has shifted north by $2\text{--}7^\circ$, on average by about 4° (from 56.6°S at PD to 52.4°S at the LGM). These values are slightly lower than the $5\text{--}8^\circ$ northward shift reported by [13]. A more recent reconstruction [14] reports a northward shift of about 5° in the Atlantic sector between 70°W and 45°E in good agreement with the simulated value (4.6°) in this region. The simulated

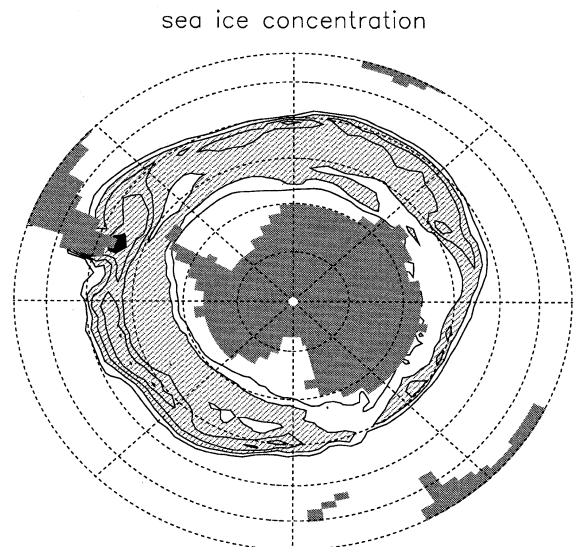


Fig. 4. Difference in annual mean sea ice concentration in the southern hemisphere between glacial and PD simulations. Contour line difference is 10% , increases between 20 and 50% are shaded, increases above 50% shaded in black.

surface ^{14}C fluxes (10^{-4}m/s)

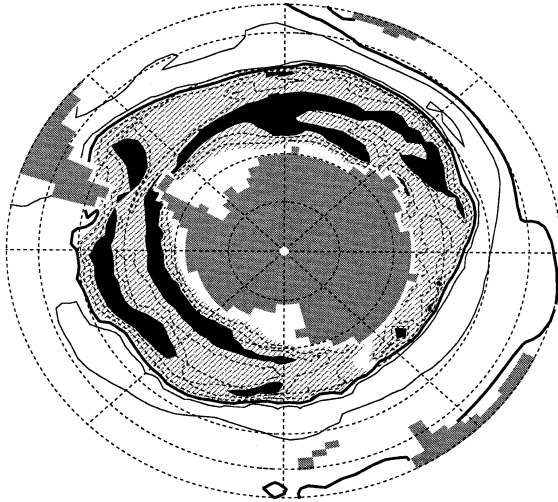


Fig. 5. Difference in air-sea fluxes of radiocarbon. Contour line differences are 0.2×10^{-4} m/s, with negative values dashed and zero line bold. Decreases of ocean uptake between 0.1 and 0.5×10^{-4} m/s are shaded, larger decreases shaded black.

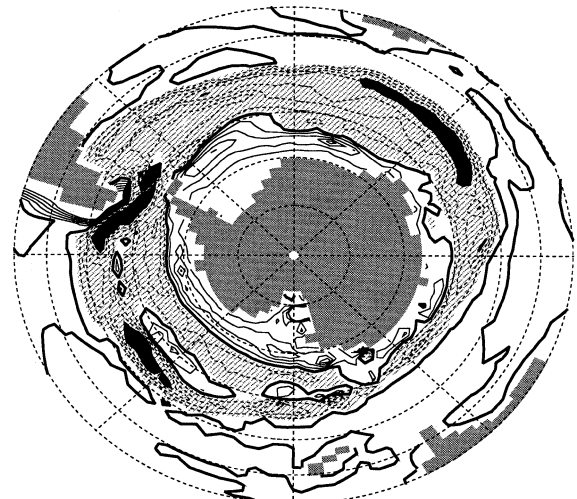
northward shift of the winter sea ice edge is only weakly dependent on the rate of NADW formation. In a simulation with absent NADW the average northward shift is slightly less (3°) due to the seesaw behavior of high northern and southern temperatures [15].

The uptake of radiocarbon by the ocean is inhibited in regions with increased sea ice extent (Fig. 5). At lower latitudes, however, ^{14}C uptake is increased. Hence, increased sea ice cover over the Southern Ocean explains much of the older deep waters in the glacial simulation (Fig. 1). These results are consistent with a previous study using an ocean-only model with prescribed sea ice and restoring surface boundary conditions [16]. Note that the actual age of a water mass, measured as the last time it was at the surface, can be different from the radiocarbon age due to sea ice shielding [16] and due to the long equilibration time (5 yr) for the air-sea gas exchange of radiocarbon. In the present paper the terms age and ventilation are used synonymously with the ^{14}C age of a water mass.

Larger sea ice concentration in the glacial simulation also has an influence on the buoyancy of

the glacial Southern Ocean. Saenko et al. [17] recently showed that freshwater transport associated with sea ice divergence from the Antarctic continent leads to salinification of high-latitude waters and determines the sites and rates of

residual freshwater fluxes (m/yr)



P-E (m/yr)

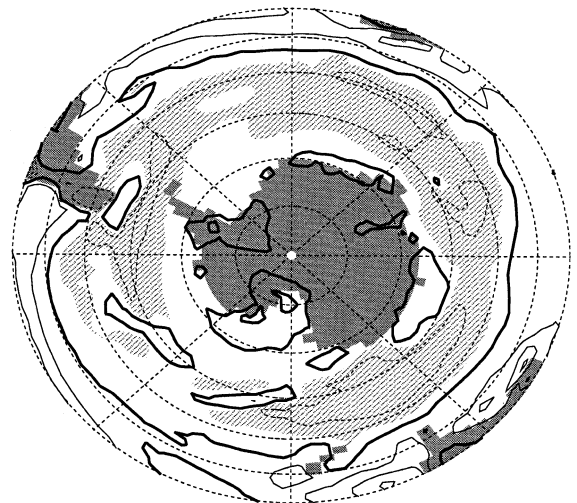


Fig. 6. (Top) Differences in surface freshwater fluxes due to changes in sea ice transport (away from continental boundaries) and runoff (at continental boundaries). Negative values correspond to increased freshwater input to the ocean, i.e. increased runoff or increased melting of sea ice. (Bottom) Differences in $P-E$. Isoline difference is 0.2 m/yr in both panels and values between -0.1 and -1 m/yr are shaded, smaller values shaded black.

AABW formation. It can be expected that this effect is enhanced in the glacial ocean, where increased sea ice coverage is likely to lead to increased meridional transport of sea ice.

The total surface freshwater flux (positive upward):

$$F = E - P - R - S$$

consists of local evaporation E and precipitation P as well as contributions from continental runoff R and convergence of sea ice S . In the equilibrium case considered here the convergence $S = m - f$ is equal to the difference between melting m and freezing f of sea ice. Subtracting $E - P$ from the total flux gives the residual freshwater flux $F_r = F - (E - P) = -(R + S)$, which only depends on runoff and sea ice transport. Runoff is non-zero only along continental boundaries. Thus away from the coast F_r is the freshwater flux due to sea ice divergence. In Fig. 6 the difference of this quantity between the glacial and PD simulations is shown together with changes in $P - E$.

Differences in sea ice transport clearly dominate changes of the Southern Ocean freshwater balance in most regions. Increased sea ice divergence from high latitudes leads to a net export of freshwater, causing the salinification of waters south of 60°S (see Fig. 3). The sea ice melts at lower latitudes, resulting in a larger freshwater input and fresher waters north of 60°S.

4. Comparison with reconstructions

A recent examination of glacial sediment porewaters also found higher salinities of southern hemisphere bottom waters [18]. In Fig. 7 the model results are compared with observed/reconstructed bottom water properties. For the present day there is a transition from relatively warm and salty NADW to fresher and colder AABW. Our model captures this transition and the relative differences in potential temperature and salinity quite well.

The reconstruction yields glacial bottom water temperatures close to the freezing point. Modeled glacial bottom water temperatures are also considerably colder than modern values. In the recon-

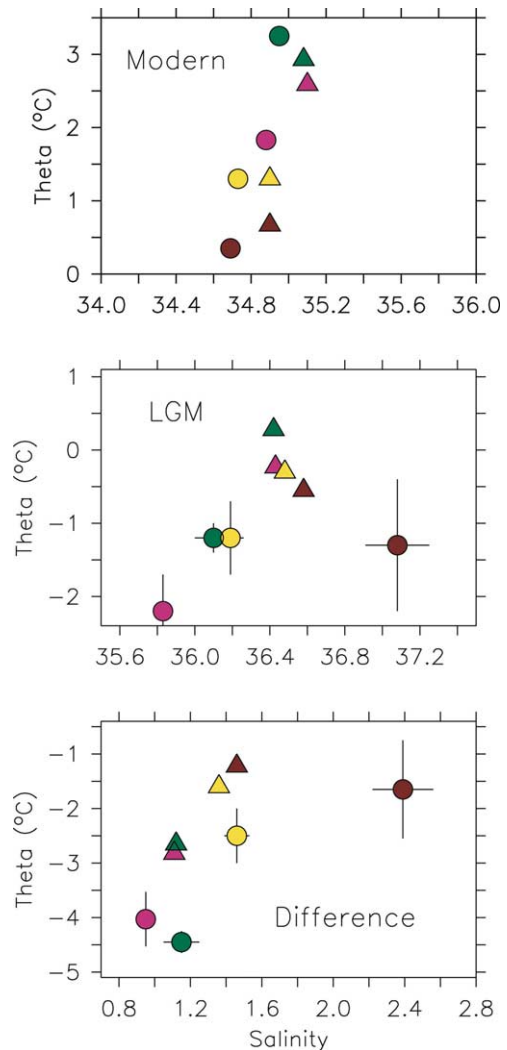


Fig. 7. Comparison of observed/reconstructed [18] (circles) and modeled (triangles) bottom water properties. Green: North Atlantic (55°N, 15°W, 2180 m); violet: North Atlantic (34°N, 58°W, 4580 m); yellow: South Pacific (42°S, 171°W, 3290 m); red: Southern Ocean (50°S, 6°E, 3630 m). Reconstructed values are shown with the published error estimates. Note: upper panels have identical ranges in theta (3.5°C) and salinity (2) while absolute values are different. The global mean salinity difference with observations [29] (0.22) is subtracted from the modern model results to remove the influence of net extraction of freshwater during the experiment (see [6]). Glacial model salinities are additionally corrected for global sea level drop by adding 1.2 salinity units. (For colors see online version of this article on <http://www.sciencedirect.com>. In the printed version green is replaced by the lightest grey and red by the darkest, with the two middle shades representing violet and yellow.)

struction as well as in the model cooling is larger for Atlantic waters and smaller for waters of southern origin. However, the simulated cooling of Atlantic bottom waters is smaller than in the reconstruction. The temperature variability between the four sites, which at PD amounts to 3°C, has decreased to only 1°C for the glacial ocean, consistently in the reconstruction and the model results.

Both reconstruction and simulation show larger salinification of AABW than NADW, such that AABW becomes the most saline bottom water mass of the glacial ocean. However, the increase is larger in the reconstruction than in the model. This leads to a larger variability in bottom water salinities in the reconstruction compared to the model. One reason for the underestimated salinity of glacial AABW could be the use of PD wind velocities in moving the sea ice. Increased wind velocities at the LGM could lead to higher rates of sea ice divergence from Antarctica and hence more saline AABW.

Comparison with other model experiments in which the rate of NADW was different did not lead to a considerably different match with the reconstructions at these four sites. Thus the bottom water data from [18] cannot be used as constraints on the rate of NADW.

No measurements of Southern Ocean radiocarbon ages seem to be available for the LGM time slice. Dating 16.5 ka before present, however, a deep sea coral from the late glacial Drake Passage at 1100 m depth could be measured. Goldstein et al. [19] find that glacial bottom waters were 200–350 yr older than modern waters. At the same site and depth the model results in an increase of 210 yr, from 1168 yr at PD to 1382 yr at the LGM (values computed with reference to atmospheric ^{14}C), consistent with the reconstruction.

Measurements of late glacial sediments from the southwest Pacific [20] show increased ventilation ages by 250 yr at 1700 m depth (as calculated by [19]). At this location the model increase (260 yr) is in agreement with the reconstruction.

Observations from older sediments in the southwest Pacific (at 177°E, 37°S and 179°E, 45°S near New Zealand) indicate much older ventilation ages. Surface water ages increase from 400 yr at

PD to 2000 yr at 22 600 ^{14}C yr BP and deep water ages from 1300–1800 yr for the PD to 3000–5000 yr [20]. In the model, surface radiocarbon ages never increase above 500 yr at these locations and deep waters do not increase above 2200 yr even for the case with fully collapsed NADW. The reason for this apparent discrepancy is not clear. The oldest surface waters in the model (1000 yr at PD, 1200–1500 yr at the LGM) are located at high southern latitudes, where perennial sea ice cover leads to an effective insulation from the atmosphere. It is unlikely that perennial sea ice covered latitudes near New Zealand and other processes leading to similar effective insulation from the air–sea exchange are difficult to imagine.

Reconstructed top-to-bottom age differences of up to 3000 yr [20] are also much larger than modeled values. Even in the case of a full collapse of NADW simulated top-to-bottom age differences never increase above 2000 yr at these locations. Large additional reductions of ventilation in the Southern Ocean and/or substantially reduced diapycnal mixing rates would be required to explain these large ventilation ages. Uncertainties in the history of atmospheric radiocarbon [21] complicate the interpretation of the very old ventilation ages of [20].

5. Uncertainties

Every modeling study is prone to systematic deficiencies due to model simplifications. Resulting uncertainties with respect to reported results are often difficult to quantify. This is also the case here. Note that a realistic simulation of the LGM ocean was not attempted. Rather, the aim of the study was to illustrate the effect of Southern Ocean sea ice on glacial bottom waters and to provide a first quantification of its magnitude. Nevertheless, in the following I attempt to estimate at least the sign towards which known model biases and simplifications affect the results.

While the simulated increase of Southern Ocean sea ice seems to agree well with reconstructions as outlined in Section 3, the total area of modeled glacial sea ice extent might be overestimated since

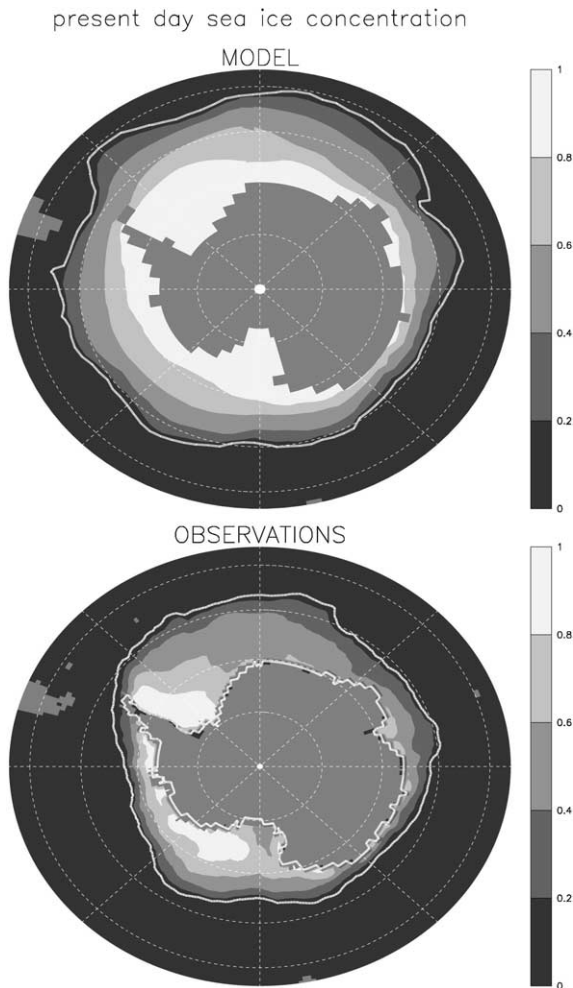


Fig. 8. Comparison of modeled annual mean sea ice concentration for PD with observations from 1987 to 1988 (Nomura and R. Grumbine, personal communication, 1995). The bold white line (0.1 isoline) gives approximate winter sea ice edge.

PD sea ice is overestimated (Fig. 8). Annual mean southern hemisphere sea ice area is overestimated in the modern simulation by a factor of two ($8.2 \times 10^6 \text{ km}^2$ in the observations versus $16.7 \times 10^6 \text{ km}^2$ in the model). This model deficiency has already been mentioned in [17] and is, inter alia, related to the underestimation of leads and polynyas and a cold bias in the atmospheric model. Sea ice volume, with $8.4 \times 10^3 \text{ km}^3$ in the model versus 10^4 km^3 estimated from observations [22], and the amplitude and timing of the seasonal

cycle [17], however, are in good agreement with PD observations.

It is conceivable that a more realistic simulation would permit larger differences between LGM and PD sea ice concentration around Antarctica and hence enhance the radiocarbon age differences of AABW. The salinification and production rate of glacial AABW would presumably also be increased.

Changes in wind are not taken into account. Increases in wind stress could lead to higher sea ice divergence and increase AABW formation rate even further. This would lead to higher salinity of southern bottom waters and an additional increase in abyssal radiocarbon ages. On the other hand, increased wind stress could increase air–sea uptake of radiocarbon if a more realistic, wind speed-dependent parameterization was considered. This would lower bottom water ^{14}C ages.

For other systematic model errors the assessment is even more difficult. Effects of high-frequency variability, a more realistic treatment of diapycnal diffusion and the inclusion of gas exchange through leads and polynyas remain to be investigated in future studies.

6. Conclusions

Using simulations of present and glacial radiocarbon distributions I have shown that increased sea ice cover over the glacial Southern Ocean leads to a considerable decrease in air–sea exchange of radiocarbon. This increases the radiocarbon age of global bottom waters by more than 100 yr. Larger off-shore sea ice transport also increases salinities and densities of AABW. These features seem to be corroborated by reconstructions of the glacial Southern Ocean.

Higher densities lead to increased down-welling rates of AABW in the model. However, despite larger fluxes of AABW the ventilation of the glacial Southern Ocean in terms of radiocarbon uptake is decreased due to insulation of the ocean from the atmosphere through increased sea ice cover. The transfer of tracers influenced by air–sea exchange to the deep ocean is therefore decoupled from the vertical mass transfer.

Older waters of southern origin are advected into other ocean basins like the Atlantic, where they increase deep water radiocarbon ages. Thus the observation of a few hundred years older deep waters in the North Atlantic [3] does not necessarily imply a reduced flux of NADW. This confirms the proviso by Wunsch [5] that inferences from tracer distributions on the mass flux are difficult and should be made with caution. However, climate models are excellent tools to quantify processes that lead to different tracer distributions and detailed comparison with reconstructions can in principle lead to constraints on the circulations [6].

At present, however, rare and conflicting reconstructions [3,12] as well as complications with some reconstructions [23] make it difficult to infer glacial mass fluxes from radiocarbon distributions. Remedy might come from an increased number of measurements on deep sea corals [19,24]. Also, combinations of different tracers simulated with the same model and subsequent comparison with available observations might prove a successful strategy to infer past ocean circulations.

The role of sea ice cover on glacial–interglacial variations of atmospheric CO₂ has recently been discussed controversially [25–27]. Assuming that reduced air–sea exchange also applies for CO₂, and considering the effect of sea ice on ocean ventilation [17,28], I speculate that increased Southern Ocean sea ice cover might have important implications for the glacial–interglacial variations of atmospheric CO₂. However, a full marine carbon cycle model has to be employed in order to investigate this subject quantitatively.

Acknowledgements

Comments from D. Roche, L. Keigwin, J.R. Toggweiler and an anonymous reviewer were appreciated. I also want to thank Oleg A. Saenko, Katrin J. Meissner and Karen E. Kohfeld for comments on an earlier version of the manuscript. Present-day sea ice observations from: http://ingrid.ldeo.columbia.edu/SOURCES/NASA/ISLSCP/GDSLAM/Snow-Ice-Oceans/.sea/.sea_ice/-data-set_documentation.html [BARD]

References

- [1] J.-C. Duplessy, N.J. Shackleton, R.G. Fairbanks, L. Labeyrie, D. Oppo, N. Kallel, Deepwater source variations during the last climate cycle and their impact on the global deepwater circulation, *Paleoceanography* 3 (1988) 343–360.
- [2] E.A. Boyle, Last-Glacial-Maximum North Atlantic Deep Water: on, off or somewhere in between?, *Philos. Trans. R. Soc. London B* 348 (1995) 243–253.
- [3] W.S. Broecker, T.-H. Peng, S. Trumbore, G. Bonani, W. Wolfli, The distribution of radiocarbon in the glacial ocean, *Glob. Biogeochem. Cycles* 4 (1990) 103–106.
- [4] P. Legrand, C. Wunsch, Constraints from paleotracer data on the North-Atlantic circulation during the Last Glacial Maximum, *Paleoceanography* 10 (1995) 1011–1045.
- [5] C. Wunsch, Determining paleoceanographic circulations, with emphasis on the Last Glacial Maximum, *Quat. Sci. Rev.* 22 (2003) 371–385.
- [6] K. Meissner, A. Schmittner, A. Weaver, J.F. Adkins, The ventilation of the North Atlantic Ocean during the Last Glacial Maximum - a comparison between stimulated and observed radiocarbon ages, *Paleoceanography* 18 (2003) 10.1029/2002PA000762.
- [7] A.J. Weaver, M. Eby, E.C. Wiebe, C.M. Bitz, P.B. Duffy, T.L. Ewen, A.F. Fanning, M.M. Holland, A. MacFadyen, H.D. Matthews, K.J. Meissner, O. Saenko, A. Schmittner, H. Wang, M. Yoshimori, The UVic Earth System Climate model: Model description, climatology, and applications to past, present and future climates, *Atmos.-Ocean* 39 (2001) 361–428.
- [8] R. Pacanowski, MOM 2 documentation user's guide and reference manual, GFDL Ocean Group Techn. Rep., NOAA, GFDL, Princeton, NJ, 1995.
- [9] P.R. Gent, J.C. McWilliams, Isopycnal mixing in ocean circulation models, *J. Phys. Oceanogr.* 20 (1990) 150–155.
- [10] J.R. Toggweiler, K. Dixon, K. Bryan, Simulation of radiocarbon in a coarse-resolution world ocean model, 2. Distributions of bomb-produced carbon 14, *J. Geophys. Res.* 94 (1989) 8243–8264.
- [11] T.F. Stocker, D.G. Wright, Rapid changes in ocean circulation and atmospheric radiocarbon, *Paleoceanography* 11 (1996) 773–796.
- [12] L.D. Keigwin, M.A. Schlegel, Ocean ventilation and sedimentation since the glacial maximum at 3 km in the western North Atlantic, *Geochem. Geophys. Geosyst.* 3, 10.1029/2001GC000283.
- [13] X. Crosta, J. Pichon, L. Burckle, Application of modern analog technique to marine Antarctic diatoms: Reconstruction of maximum sea-ice extent at the Last Glacial Maximum, *Paleoceanography* 13 (1998) 284–297.
- [14] R. Gersonde, A. Abelmann, U. Brathauer, S. Bequey, C. Bianchi, G. Cortese, H. Grobe, G. Kuhn, H.-S. Niebler, M. Segl, R. Siegler, U. Zielinski, D.K. Fütterer, Last glacial sea-surface temperatures and sea-ice extent in the

- Southern Ocean (Atlantic-Indian sector) - a multi-proxy approach, *Paleoceanography* (2003) in press.
- [15] A. Schmittner, O.A. Saenko, A.J. Weaver, Coupling of the hemispheres in observations and simulations of glacial climate change, *Quat. Sci. Rev.* 22 (2003) 659–671.
- [16] J.-M. Campin, T. Fichefet, J.-C. Duplessy, Problems with using radiocarbon to infer ocean ventilation rates for past and present climates, *Earth Planet. Sci. Lett.* 165 (1999) 17–24.
- [17] O.A. Saenko, A. Schmittner, A.J. Weaver, On the role of wind-driven sea-ice motion on ocean ventilation, *J. Phys. Oceanogr.* 32 (2002) 3376–3395.
- [18] J.F. Adkins, K. McIntyre, D.P. Schrag, The salinity, temperature and $\delta^{18}\text{O}$ of the glacial deep ocean, *Science* 298 (2002) 1769–1773.
- [19] S.J. Goldstein, D.W. Lea, S. Chakraborty, M. Kashgarian, M.T. Murrell, Uranium-series and radiocarbon geochronology of deep-sea corals: implications for Southern Ocean ventilation rates and the oceanic carbon cycle, *Earth Planet. Sci. Lett.* 193 (2001) 167–182.
- [20] E.L. Sikes, C.R. Samson, T.P. Guilderson, W.R. Howard, Old radiocarbon ages in the southwest Pacific Ocean during the last glacial period and deglaciation, *Nature* 405 (2000) 555–559.
- [21] J.W. Beck, D.R. Richards, R.L. Edwards, B.W. Silverman, P.L. Smart, D.J. Donahue, S. Herrera-Osterheld, G.S. Burr, L. Calsoyas, A.J.T. Jull, D. Biddulph, Extremely large variations of atmospheric ^{14}C concentrations during the last glacial period, *Science* 292 (2001) 2453–2458.
- [22] J.W. Weatherly, T.W. Bettge, W.M. Washington, Simulation of sea-ice in the NCAR Climate System Model, *Ann. Glaciol.* 25 (1997) 107–110.
- [23] W.S. Broecker, K. Matsumoto, E. Clark, I. Hajdas, G. Bonani, Radiocarbon age differences between coexisting foraminiferal species, *Paleoceanography* 14 (1999) 431–436.
- [24] A. Mangini, M. Lomitschka, R. Eichstädter, N. Frank, S. Vogler, Coral provides way to age deep water, *Nature* 392 (1998) 347–348.
- [25] H. Gildor, E. Tziperman, J.R. Toggweiler, Sea ice switch mechanism and glacial-interglacial CO_2 variations, *Glob. Biogeochem. Cycles* 16 (2002) 10.1029/2001GB001446.
- [26] D.E. Archer, P.A. Martin, J. Milovich, V. Brovkin, G.-K. Plattner, C. Ashendel, Model sensitivity in the effect of antarctic sea ice and stratification on atmospheric pCO_2 , *Paleoceanography* 18 (2003) 10.1029/2002PA000760.
- [27] B.B. Stephens, R.F. Keeling, The influence of Antarctic sea ice on glacial-interglacial CO_2 variations, *Nature* 404 (2000) 171–174.
- [28] J.R. Toggweiler, Variation of atmospheric CO_2 by ventilation of the ocean's deepest water, *Paleoceanography* 14 (1999) 571–588.
- [29] S. Levitus, R. Burgett, T.P. Boyer, NOAA Atlas NESDIS 3, World Ocean Atlas 1994, Vol. 3: Salinity, NOAA, U.S. Dept. Commerce, 1994, 99 pp.